Time-Resolved Small-Angle Neutron Scattering in Intermediate- and Late-Stage Spinodal Decomposition of DPB/HPI Blends

Hiroshi Jinnai, Hirokazu Hasegawa, and Takeji Hashimoto*

Department of Polymer Chemistry, Kyoto University, Kyoto 606, Japan

Charles C. Han

Polymers Division, National Institute of Standards and Technology, Gaithersburg, Maryland 20899

Received May 2, 1990; Revised Manuscript Received June 21, 1990

ABSTRACT: Time-resolved small-angle neutron scattering (SANS) experiments were performed to study the later stage (i.e., the intermediate stage and the late stage) of spinodal decomposition (SD) of a critical mixture of perdeuterated polybutadiene (DPB) and protonated polyisoprene (HPI) with an LCST-type phase diagram and a critical temperature T_c = 36.1 °C. Time-sliced SANS intensity, $S(q,t)$, is generally composed of the scattering due to growing domains, $I_d(q,t)$, and that due to the thermally induced local composition fluctuations inside the domain $I_T(q,t)$ where q and t are the scattering vector and time, respectively. $S(q,t)$ as a function of q shows the "spatial crossover" such that at q much below and above a time-dependent wavenumber, $q_s(t)$, it depends only on $I_d(q,t)$ and $I_T(q,t)$, respectively. The time evolution of the composition difference between the two coexisting domains, $\Delta\Phi(t)$, was determined from $I_T(q,t)$, which was found to be consistent with the prediction of the scattering theory based upon the random-phase approximation. $\Delta\Phi(t)$ was found to increase with t and reach a constant equilibrium value $\Delta\Phi_e$ at $t > t_{cr}$, where t_{cr} is the crossover time from the intermediate to the late-stage SD. The crossover wavenumber, $q_s(t)$, also underwent a characteristic change at t_{cr}.

I. Introduction

Recently many studies have been made on the kinetics of phase separation of polymer blends in the early-stage spinodal decomposition (SD).[1] Self-assembling processes, patterns (morphology), and dynamics in the later stage SD have also been investigated[1] as a problem of nonequilibrium statistical mechanics of long-chain molecules. Here the later stage SD refers to the intermediate stage and the late stage of SD.[2] In most of the experimental studies along these lines, time-resolved light-scattering (LS) methods[1-5] were used, but time-resolved small-angle neutron scattering (SANS)[6-10] and small-angle X-ray scattering (SAXS) methods[11-13] were used in only a few studies.

Concerning the studies in the later stage SD, the dynamical scaling hypothesis has been critically tested. Whether the growing global structure of the self-assembling structure can be scaled with a single time-dependent length parameter, $\Lambda_m(t)$, has been efficiently tested by time-resolved LS.[2,14-17] There still remains an important question: whether the local structure, e.g., interfacial structures including waviness of the interface and interfacial width, can also be scaled with $\Lambda_m(t)$.[15] In fact the scaled structure factor in the late-stage SD as observed by time-resolved LS shows a fine structure at large wavenumber q satisfying $q > 2q_m \equiv 4\pi/\Lambda_m(t)$.[15,17-20] Moreover, in some cases the scaled structure factor is nonuniversal at large q, and hence the time evolution of the interfacial structure cannot be scaled with $\Lambda_m(t)$.[15,21] Time-resolved SANS and SAXS are useful methods to investigate the time evolution of the interfacial structure as they can approach a much shorter length scale than LS.

This paper describes the time evolution of composition difference between two coexisting domains, $\Delta\Phi(t)$, in the later stage SD. This is the first report of this series, the aim of which is to investigate the time evolution of the interfacial structure using time-resolved SANS and LS on the same blend specimens.

We characterized the mixture in the single-phase state (section III-1). We critically tested the theoretical prediction of the random-phase approximation (RPA)[22] on thermally induced local composition fluctuations, as the theory is extensively applied to analyze the time-resolved SANS results (section III-2). We discussed the general trends on the time change of SANS profiles, $S(q,t)$ (section IV-1), the crossover behavior of $S(q,t)$ from "domain scattering" to "internal scattering" (i.e., the scattering due to local composition fluctuations within each domain) with increasing q through the crossover wavenumber, $q_s(t)$ (section IV-2), and determination of $\Delta\Phi(t)$ as well as the time change of $\Delta\Phi(t)$ and $q_s(t)$ (section IV-3).

II. Experimental Section

1. Samples. Perdeuterated polybutadiene (DPB) (coded as H18) and protonated polyisoprene (HPI) (coded as H15) used in this study were synthesized by living anionic polymerization. Table I summarizes the polymer characteristics. Note that these two polymers are very symmetric in terms of molecular weight, density, and Kuhn's statistical segment length. Hence, the blend has a symmetric phase diagram.

2. Test Specimens for SANS Experiments. Film specimens of a DPB/HPI blend (50/50 wt %/wt % or 51/49 vol %/vol %) were prepared by dissolving DPB and HPI into a homogeneous toluene solution of approximately 5 wt % total polymer concentration. The solution was cast into a thin film of about 0.15 mm thick in a Petri dish. The as-cast films thus obtained were further dried in a vacuum oven at room temperature until constant weight was attained. The thin as-cast films were pressed in the cell to make thicker disk-shaped specimens. The disk-shaped specimens prepared for all SANS experiments were about 1 mm thick and about 13 mm in diameter and were carefully degassed under vacuum in order to avoid bubble formation in the specimens during heating experiments and then put between two oxygen-free pure copper disks about 0.22 mm thick with a ring spacer of about 1 mm thick.

The composition of the blend was very close to the critical composition predicted by Flory-Huggins, the critical volume fraction of DPB, $\phi_{c,DPB}$ being 0.52.

3. Time-Resolved SANS Experiments. SANS experiments were carried out at the NIST Research Reactor.[23] In this study,

0024-9297/91/2224-0282$02.50/0

Table I
Polymer Characteristics

specimen code	$\bar{M}_n \times 10^{-3}$ [a]	$\bar{M}_w/\bar{M}_n$ [a]	$\bar{N}_n$ [b]	microstructure,[c] % 1,2	cis-1,4	trans-1,4	3,4
H15(HPI)	136	1.0_4	2000	0	63	22	15
H18(DPB)	103	1.0_3	1717	20	36	44	0

[a] Determined by size-exclusion chromatography with light scattering. [b] Number-averaged degree of polymerization. [c] Determined by ^{13}C NMR.

Table II
Characterization of Blend

(1) phase diagram: LCST
(2) blend composition, DPB/HPI: 50/50 wt %/wt % or 51/49 vol %/vol %
(3) critical volume fraction of DPB calculated from Flory–Huggins theory: $\Phi_{c,DPB} = 0.52$
(4) unperturbed radius of gyration: $R_g = 11.1$ nm for DPB, 12.0 nm for HPI
(5) spinodal temperature T_s measured by SANS: $T_s = 36.1$ °C
(6) Flory χ-parameter as determined from SANS profiles in the single-phase state: $\chi = 6.77 \times 10^{-3} - 1.75/T$
(7) quench depth ΔT_s and $\epsilon_T = (\chi - \chi_s)/\chi_s$ for time-resolved SANS experiments (χ_s; χ-parameter at T_s): $\Delta T_s = 3.9$ K, $\epsilon_T = 0.0668$
(8) wavenumbers $q_m(0)$ and $q_c = \sqrt{2}q_m(0)$ in the early-stage SD predicted by Cahn's theory: $q_m(0) = 0.027$ nm^{-1}, $q_c = 0.039$ nm^{-1}

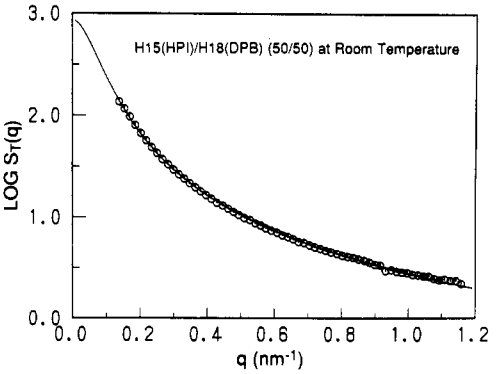

Figure 1. Typical SANS profile of a H15(HPI)/H18(DPB) blend obtained at room temperature (circles) and the best fitted theoretical profile (solid line).

the focusing optical geometry was used with an 11-Å neutron wavelength. The spectral resolution $\Delta\lambda/\lambda$ was 0.25 where λ is the wavelength of the neutron beam. The observed scattering intensity was corrected for electronic noise, background radiation, and detector inhomogeneity. It was then normalized against dry silica gel, which serves as a secondary standard, to give the absolute intensity.[24]

A copper block with heating elements was used to control the temperature of the specimens within ±0.3 °C during SANS measurements. Temperature-jump (T-jump) experiments were carried out by manually transferring the specimen at room temperature (23 °C) into the copper block preheated and controlled at the measuring temperature (40 °C). It took about 1–2 min for the specimen to attain the measuring temperature after the T-jump.

A time-resolved SANS profile at a given time t was measured for a time period of t and t + PT where the preset time, PT, was fixed to 3 min in this study. The SANS profiles were measured with a two-dimensional detector at a sample-to-detector distance of 3.6 m and the circularly averaged corrected intensity, $S(q,t)$, was subjected to further analyses where q is the magnitude of scattering vector as defined by

$$q = (4\pi/\lambda) \sin(\theta/2) \tag{1}$$

θ is the scatterng angle.

III. Characterization of the Mixture in the Single-Phase State

We analyzed the static SANS profiles, $S_T(q)$, at various temperatures in the single-phase state to determine the Flory interaction parameter per monomeric unit as a function of temperature T, $\chi(T)$, and spinodal temperature, T_s, for the critical mixture of DPB/HPI in section III-1. Table II summarizes the results of the characterization of the mixture. We have critically tested the RPA predictions on thermally induced local composition fluctuations by comparing theoretical and experimental $S_T(q)$ at large q, which will be presented in section III-2. This is necessary because we applied the RPA theory for $S_T(q)$ to the analyses of the time-resolved SANS data on $S(q,t)$ at large q in section IV-2 and -3.

1. Spinodal Temperature and $\chi(T)$. We measured $S_T(q)$ at various temperatures in the single-phase state. Figure 1 shows an example of $S_T(q)$ at 23 °C where the profiles shown by circles and a solid line indicate, respectively, the experimental and the best fitted theoretical profile. The theoretical $S_T(q)$ derived by RPA for blends of an asymmetric pair of polymers A and B is given by

$$\left[\frac{S_T(q)}{k_N}\right]^{-1} = \frac{1}{N_A\phi_A v_A G_D(X_A)} + \frac{1}{N_B\phi_B v_B G_D(X_B)} - \frac{2\chi}{v_0} \tag{2}$$

where N_K, ϕ_K, v_K, and $G_D(X_K)$ are, respectively, the degree of polymerization, the volume fraction, the monomeric molecular volume, and Debye's scattering function of a single Gaussian coil for polymer K (K = A or B), and k_N is the contrast factor, which can be written as

$$k_N = N_0(b_A/v_A - b_B/v_B)^2 \tag{3}$$

with b_K as the scattering length of one monomeric unit of polymer K and N_0 as Avogadro's number. v_0 is the cell volume, which is assumed to be given by

$$v_0 = (\phi_A/v_A + \phi_B/v_B)^{-1} \tag{4}$$

and X_K is defined as

$$X_K = q^2 R_{gK}^2 = q^2(N_K a_K^2/6) \tag{5}$$

where R_{gK} is the unperturbed radius of gyration and a_K is Kuhn's statistical segment length of polymer K.

The best fitting procedure[25] yielded information on χ and the zero-wavenumber scattering intensity, $S_T(0)$. Temperature dependencies of χ and $S_T(0)^{-1}$ thus determined by the best fittings at various T's were plotted in Figure 2 where χ was found to be given by

$$\chi = 6.77 \times 10^{-3} - 1.75/T \tag{6}$$

From eq 2, $S_T(0)^{-1}$ and ξ^{-2} (ξ being the thermal correlation length[22]) are given by

$$S_T(0)^{-1} \sim (\chi_s - \chi) \tag{7}$$

and

$$\xi^{-2} = 36\phi_A(1 - \phi_A)(\chi_s - \chi)/a^2 \tag{8}$$

where χ_s is the χ-parameter at T_s and a_K's were assumed

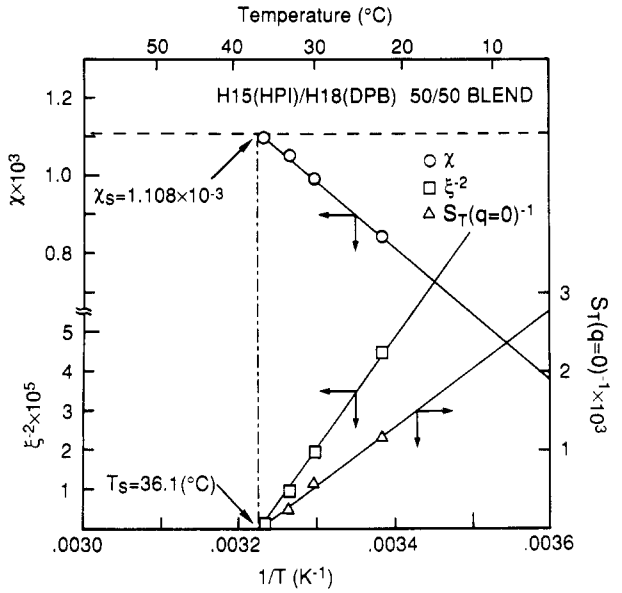

Figure 2. Flory interaction parameter per monomeric unit, χ, reciprocal zero-wavenumber scattering intensity, $S_T(0)^{-1}$, and reciprocal squared thermal correlation length, ξ^{-2}, as a function of $1/T$ obtained for a H15(HPI)/H18(DPB) blend.

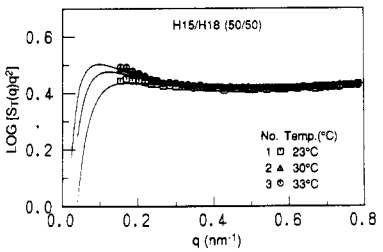

Figure 3. Semilogarithmic plot of $S_T(q)\ q^2$ vs q for a H15/H18 (50/50) blend at 23 °C (□), 30 °C (△) and 33 °C (○). The solid lines show the theoretical curves.

to be equal to a. Since χ is linear with $1/T$, $S_T(0)^{-1}$ and ξ^{-2} are also expected to be linear with $1/T$. In fact, $S_T(0)^{-1}$was found to be linear with $1/T$ and became zero at T_s = 36.1 °C (Figure 2). This T_s value was inserted into eq 6, and χ_s was evaluated. When this χ_s value and $\chi(T)$ given by eq 6 were used together with eq 8, ξ^{-2} was evaluated as a function of $1/T$, the result of which was also included in Figure 2.

2. Test of RPA Prediction on Local Composition Fluctuations. From eq 2

$$I_T^e(q) \equiv \lim_{q\to\infty}[S_T(q)/k_N] = [12\phi_A(1-\phi_A)/\langle a^2/v\rangle]q^{-2}\ (\text{at } q \gg 1/R_g) \quad (9)$$

where

$$\langle a^2/v\rangle \equiv (a_A^2/v_A)(1-\phi_A) + (a_B^2/v_B)\phi_A \quad (10)$$

$I_T^e(q)$ is the scattering due to thermally induced local composition fluctuations occurring at a length scale much shorter than R_{gK} or at q much larger than $1/R_{gK}$. It has a q^{-2} dependence, the prefactor of which also depends on the local composition of ϕ_K but not on χ and hence not on T. Figures 3 and 4 show the results of the experimental tests of this prediction.

Figure 3 shows log $[S_T(q)q^2]$ as a function of q for the critical mixture of DPB/HPI at three temperatures where the solid lines show the theoretical curves calculated from eq 2 with parameters N_K, a_K, v_K, and v_0 as described earlier. The results indicated that the RPA theory predicts well the scattering $I_T^e(q)$ at the large q limit. The theory

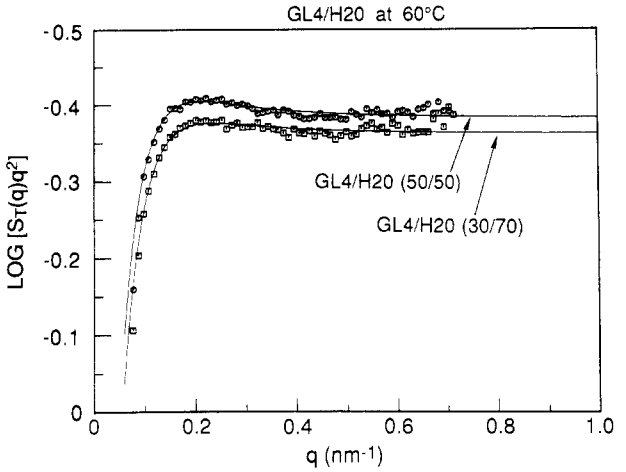

Figure 4. Semilogarithmic plot of $S_T(q)\ q^2$ vs q for GL4(HPI)/H20(DPB) (50/50) and (30/70) blends. The solid lines show the theoretical curves.

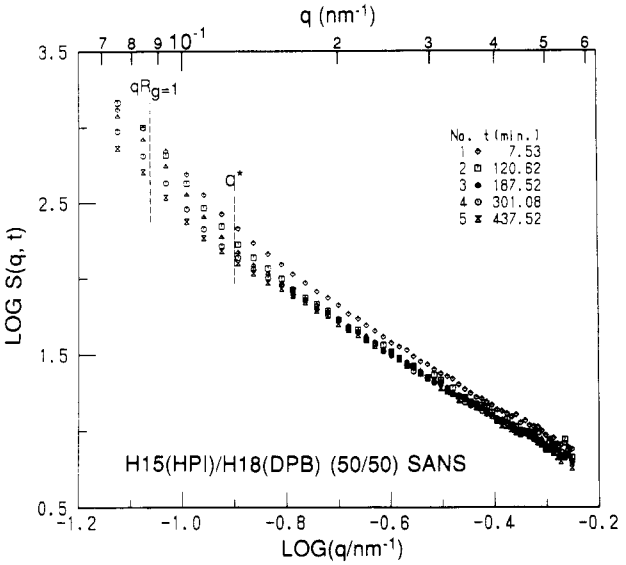

Figure 5. Time change of SANS scattering profiles after the T-jump from 23 to 40 °C for a H15(HPI)/H18(DPB) (50/50) blend.

describes well the composition dependence of $I_T^e(q)$ also as shown in Figure 4 where log $[S_T(q)q^2]$ was plotted as a function of q for DPB/HPI mixtures, which had a composition of 50/50 and 30/70 wt %/wt % at 60 °C. The RPA predictions are shown by the solid lines. Different HPI(GL4) and DPB(H20) were used here; their 50/50 and 30/70 mixtures had T_s = 96.0 and 111.2 °C, respectively. GL4 has the characteristics $M_n = 1.0 \times 10^5$, M_w/M_n = 1.01, and the content of 1,2-, cis-1,4, trans-1,4, and 3,4-linkages as 0, 69, 24, and 7%, respectively, and H20 has $M_n = 5.9 \times 10^4$, M_w/M_n = 1.07, and the content of 1,2-, cis-1,4, trans-1,4, and 3,4-linkages as 16, 38, 46, and 0%, respectively. These results on $I_T^e(q)$ will be extensively applied to further analyses of the time-resolved scattering profiles, $S(q,t)$, in the next section.

IV. Results on Time-Resolved SANS and Discussion

1. General Trend. Figures 5–7 show the general trend on time change of the SANS scattering profile, $S(q,t)$, for the critical mixture of HPI(H15)/DPB(H18) after the T-jump from 23 to 40 °C. As shown in Figure 5 the time change of $S(q,t)$ is rather monotonous, compared with that in the small q-regime as observed by LS.[21] The time

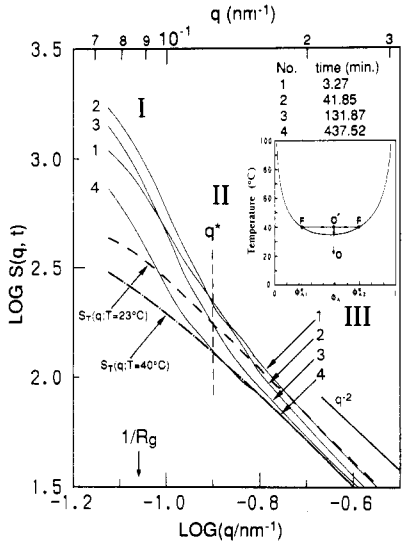

Figure 6. Double-logarithmic plot of $S_T(q,t)$ vs q for a H15(HPI)/H18(DPB) (50/50) blend after the T-jump from 23 to 40 °C (solid lines). The broken line and dash-dot line correspond, respectively, to the measured profile $S_T(q;T=23\ °C)$ (at a state O) for the thermal composition fluctuations before the T-jump and the theoretical profile $S_T(q;T=40\ °C)$ (at a state F) for the thermal composition fluctuations in the two macroscopic phases 1 and 2 with the volume fractions of the A polymer, ϕ_{A1}^e and ϕ_{A2}^e, at thermal equilibrium as shown in the inserted diagram.

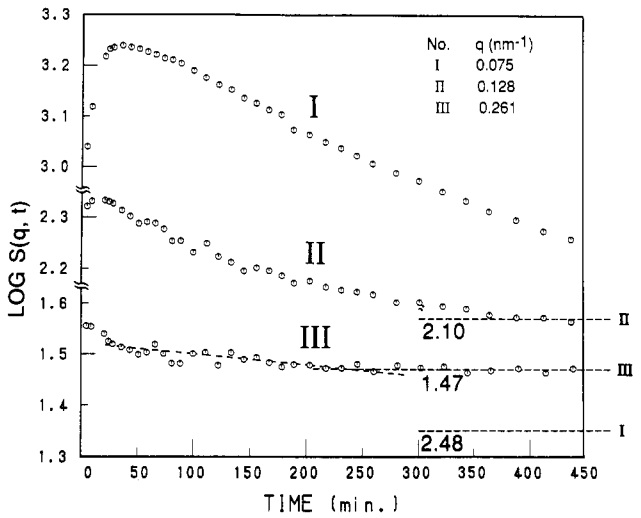

Figure 7. Time change of $S(q,t)$ in regimes I (q = 0.075 nm^{-1}), II (q = 0.128 nm^{-1}), and III (q = 0.261 nm^{-1}) for H15(HPI)/H18(DPB) (50/50) blend after the T-jump from 23 to 40 °C. The horizontal broken lines and the numbers indicate the levels of log $S_T(q;T=40\ °C)$, i.e., the levels which $S(q,t)$ are expected to attain at the two-phase equilibrium.

change of the LS profile $S(q,t)$ ($0 < q$ (nm^{-1}) < 0.01) was more dramatic on the same time scale and under the same experimental condition as that of the SANS profile; a scattering maximum appeared, the maximum intensity increased with time by about 3 orders of magnitude, and the position of the maximum in q (q_m) shifted toward smaller q's. The value $q_m = 5.5 \times 10^{-3}$ nm^{-1} was observed at t = 432.80 min, corresponding to the characteristic length of the periodic domain structure, $\Lambda_m = 2\pi/q_m = 1.14\ \mu$m. On the other hand, $S(q,t)$ in the SANS q-regime did not show either a scattering maximum or a big change in intensity, the largest intensity change observed being a factor of about 0.31 at $q = 7.6 \times 10^{-2}$ nm^{-1}.

Figure 5 includes the position of q satisfying $qR_g = 1$ where R_g is an arithmetic average of the R_g's for DPB and HPI (Table II). Thus our SANS experiments are concerned with the time change of the composition fluctuations at a length scale of R_g during the later stage of SD. At this stage it is worthwhile to note the characteristic wavenumbers $q_m(0)$ and q_c as predicted by Cahn's linearized theory.[26] The crossover wavenumber, q_c, where the growth rate, $R(q)$, of the composition fluctuations changes sign with increasing q is given by

$$q_c = 1/\xi = (\sqrt{3}/R_g)\epsilon_T^{1/2} = 0.039\ \text{nm}^{-1} \quad (11)$$

where

$$\epsilon_T = (\chi - \chi_s)/\chi_s \quad (12)$$

q_c was estimated to be 0.039 nm^{-1}, by using $\chi(T)$ measured in the single-phase state and extrapolating it to the phase-separation temperature (40 °C) ($\chi = 1.18 \times 10^{-3}$ at 40 °C), together with the estimated χ_s value ($\chi_s = 1.11 \times 10^{-3}$). The wavenumber of the dominant mode of the composition fluctuations $q_m(0)$ is given by

$$q_m(0) = q_c/\sqrt{2} = 0.027\ \text{nm}^{-1} \quad (13)$$

These wavenumbers $q_m(0)$ and q_c exist below the smallest q achieved in our SANS experiments (see Figure 6).

Figure 6 shows a closeup of $S(q,t)$ centered at log $q \cong -0.9$ and includes the measured profile of $S_T(q;T=23\ °C)$ (broken line) for the thermal composition fluctuations before the T-jump and the theoretical profile of $S_T(q;T=40\ °C)$ for the thermal composition fluctuations occurring in the two macroscopic phases 1 and 2 with the volume fractions of A polymer ϕ_{A1}^e and ϕ_{A2}^e, respectively, at thermal equilibrium as shown in the inserted diagram. $S_T(q;T=40\ °C)$ was calculated assuming

$$S_T(q,T=40\ °C) = X_1^e S_{T1}(q;T=40\ °C) + X_2^e S_{T2}(q;T=40\ °C) \quad (14)$$

where X_1^e and X_2^e are the volume fractions of the phases 1 and 2, respectively, at thermal equilibrium, $X_1^e + X_2^e = 1$. $S_{TK}(q)$ (K = 1 or 2) is the scattering intensity for the composition fluctuations in the phase K with the volume fractions of A and B polymers ϕ_{AK}^e and ϕ_{BK}^e, respectively. There is the following relationship

$$(\phi_{A2}^e - \phi_A^0)/(\phi_A^0 - \phi_{A1}^e) = X_1^e/X_2^e \quad (15)$$

ϕ_A^0 is the volume fraction of the A polymer in the initial state O. The equilibrium volume fractions of the A polymer, ϕ_{AK}^e, in the two macroscopic phases were determined by Flory–Huggins theory.

The time change of $S(q,t)$ may be classified into three regimes, i.e., regime I at $q < q^*$, regime II at $q \cong q^*$ (crossover regime), and the regime III at $q > q^*$. Comparison of $S(q,t)$ at an earlier time of SD, e.g., profiles number 1 and 2, reveals that $S(q,t)$ increases, stays constant, and decreases with t in regimes I–III, respectively. However, the observed crossover $q^* \cong 0.128$ nm^{-1} is much larger than q_c predicted by Cahn.[26] The initial increase of $S(q,t)$ with t in regime I is due to the buildup of the composition fluctuations in the early-stage SD. The decrease of $S(q,t)$ with a further elapse of t in regimes I and II is due to the coarsening of the phase-separating domains in the later stage. Here in this time period the domain size $\Lambda_m(t)$ grows with t, causing a shift of $q_m(t) = 2\pi/\Lambda_m(t)$ for the scattering peak due to the domains toward smaller q. This, in turn, causes the scattering intensity from the domain at large q-tail to decrease. The intensity $S(q,t)$ in regime III decreases with t, which implies that the local volume fraction of the A polymer, ϕ_A, is being biased with t from 0.49 in the initial state O toward ϕ_{A1}^e

and ϕ_{A2}^e in the final state F. Here the intensity is shown to decrease with t from $S_T(q;T=23\ °C)$ to $S_T(q;T=40\ °C)$.

The time change of $S(q,t)$ in different regimes is shown more explicitly in Figure 7 where log $S(q,t)$ at three representative q's is plotted as a function of t. In all cases the intensity is shown to decay eventually to the level of $S_T(q;T=40\ °C)$ relevant to the thermal composition fluctuations at the two-phase equilibrium. The horizontal broken lines and the corresponding numbers indicate the levels of log $S_T(q;T=40\ °C)$ at the three different q's numbered I–III. For curve II at $q = 0.128\ nm^{-1}$, $S(q,t)$ reaches $S_T(q;T=40\ °C)$ at the long time limit of this plot whereas it reaches the level at much shorter time for the curve III at $q = 0.261\ nm^{-1}$.

2. Spatial and Dynamical Crossover from Domain Scattering, $I_d(q,t)$, to Internal Scattering, $I_T(q,t)$. Figure 6 showed that at any given times $S(q,t)$ can be decomposed into two contributions: (i) the time-dependent scattering from the growing domains, $I_d(q,t)$, and (ii) that from the local composition fluctuations, $I_T(q,t)$

$$S(q,t) = I_d(q,t) + I_T(q,t) \tag{16}$$

At $q \ll q^*$, $I_d(q,t) \gg I_T(q,t)$; hence, $S(q,t)$ arises primarily from the domains, $I_d(q,t)$ (hereafter defined as "domain scattering"), whereas at $q \gg q^*$ (typically log $q > -0.7$ in Figure 6) $I_T(q,t) \gg I_d(q,t)$; hence, $S(q,t)$ arises primarily from the local composition fluctuations within each domain, $I_T(q,t)$ (hereafter defined as "internal scattering"). Moreover, $I_T(q,t) \sim q^{-2}$, and the prefactor depends on time-dependent compositions $\phi_{A1}(t)$ and $\phi_{A2}(t)$ in domains 1 and 2. Thus the scattering behavior shows a crossover from the domain scattering to the internal scattering with increasing q ("spatial crossover" in scattering behavior).

At a given q satisfying $q < q^*$, $I_d(q,t)$ dominates $I_T(q,t)$ at earlier times, but the former is eventually outweighed by the latter as expected again from Figure 6 ("dynamical crossover" in scattering behavior). Curve III in Figure 7 was obtained at $q = 0.261\ nm^{-1}$ (log $q = -0.583$) in regime III, so that $S(q,t)$ depends on $I_T(q,t)$

$$I_T(q,t) = f(t)\, q^{-2} \tag{17}$$

where $f(t)$ depends on the time-dependent local compositions $\phi_{A1}(t)$ and $\phi_{A2}(t)$ in the domains 1 and 2 (eq 9). At $t > 250$ min, $S(q,t)$ and hence $f(t)$ reach constant values, which implies that $\phi_{A1}(t)$ and $\phi_{A2}(t)$ reach the equilibrium values ϕ_{A1}^e and ϕ_{A2}^e, respectively. Thus the composition difference between the two domains $\Delta\Phi(t) = |\phi_{A2}(t) - \phi_{A1}(t)|$ reaches an equilibrium value $\Delta\Phi_e$ at $t > t_{cr} \cong 250$ min where t_{cr} is the crossover time from the intermediate-stage SD to the late-stage SD.[2] At $t < t_{cr}$, $\Delta\Phi(t)$ increases, or $\phi_{A1}(t)$ ($\phi_{A2}(t)$) decreases (increases) from ϕ_A^0, the initial composition, and hence $S(q,t)$ decreases with t. The decrease in $S(q,t)$ for the curves I and II in Figure 7 is due to the decrease of $I_d(q,t)$ and $I_T(q,t)$, the former contribution being expected to be substantially larger than the latter.

Figure 8 shows the time change of SANS profile, $S(q,t)$, in the early-, intermediate-, and late-stage SD where logarithms of $S(q,t)$ were plotted as a function of log q. The figure includes also $S_T(q;T=23\ °C)$ (broken lines) and $S_T(q;T=40\ °C)$ (solid lines). The time period for the early-stage SD was determined approximately as that where log $S(q,t)$ at q's in the regime I of Figures 6 and 7 increased linearly with t. In this time period the fluctuations are expected to grow approximately in the manner described by Cahn's linearized theory,[26] although the present data are not sufficient for the quantitative analyses. The three representative profiles at t = 3.27, 15.28, and 34.32 min

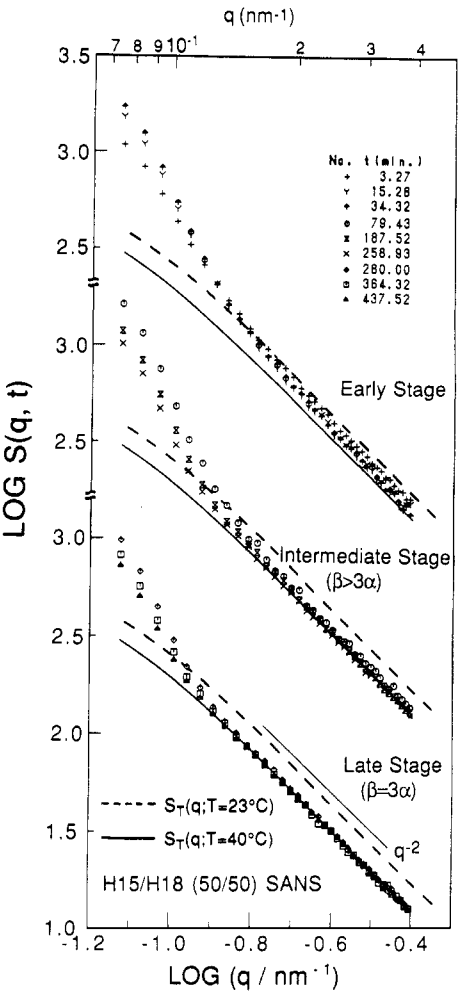

Figure 8. Time change of SANS profiles (double-logarithmic plot) in the early, intermediate-, and late-stage SD for H15(HPI)/H18(DPB) (50/50) blend after the T-jump from 23 to 40 °C. $S_T(q;T=23\ °C)$ and $S_T(q;T=40\ °C)$ are shown by broken and solid lines, respectively.

in Figure 8 belong to this time period.

The intermediate-stage and the late-stage SD were determined by time-resolved LS studies separately carried out for the same specimen under the same experimental conditions.[21] In the intermediate-stage SD,[2] $q_m(t)$ decreases or $\Lambda_m(t)$ increases with t, so that the scaling exponents α and β on $q_m(t)$ and $I_m(t)$, the time change of the maximum LS intensity, satisfy $\beta > 3\alpha$ where

$$q_m(t) \sim t^{-\alpha} \tag{18}$$

and

$$I_m(t) \sim t^{\beta} \tag{19}$$

On the other hand, in the late-stage SD[2] $\Delta\Phi(t)$ reaches $\Delta\Phi_e$ and the domains grow with dynamical self-similarity, $S(q,t)$ being scaled with a single length parameter $1/q_m(t)$. Hence, we have $\beta = 3\alpha$. The three curves at t = 79.43, 187.52, and 258.93 min in Figure 8 represent $S(q,t)$ in the intermediate stage, whereas the three curves at t = 280.00, 364.32, and 437.52 min represent $S(q,t)$ in the late stage.

Systematic change of $S(q,t)$ with t in Figure 8 clearly confirms the following two effects as discussed earlier: (i) the intensity level of q^{-2} (i.e., $f(t)$ in eq 17) systematically decreases with t in the early- and intermediate-stage SD and reaches a constant value in the late-stage SD; (ii) the crossover q (defined hereafter as q_s), above which the

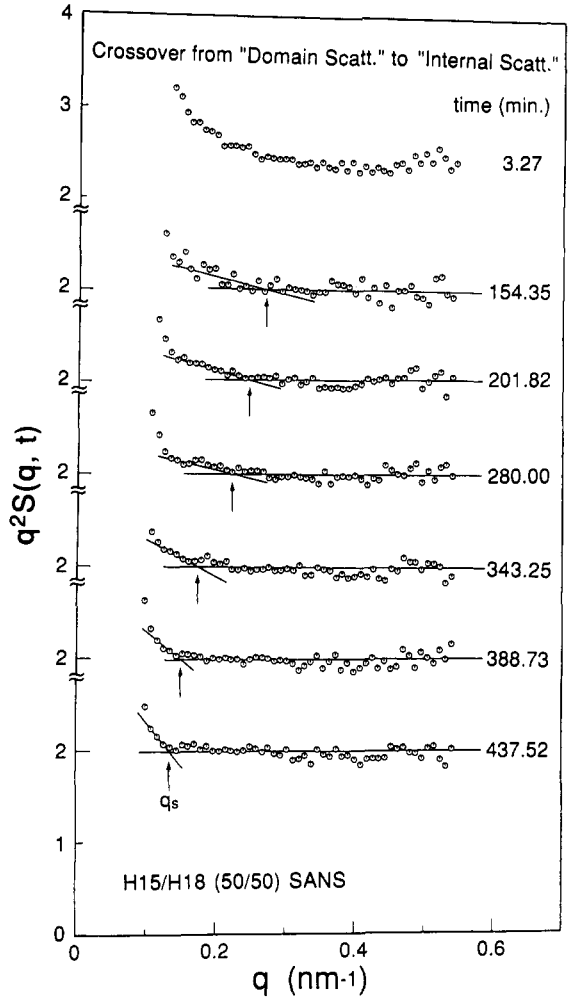

Figure 9. Plot of $q^2S(q,t)$ vs q for H15(HPI)/H18(DPB) (50/50) blend at various times after T-jump from 23 to 40 °C. The crossover q_s is indicated by an arrow.

following relationship is satisfied

$$S(q,t) = I_T(q,t) \text{ [at } q > q_s(t)] \tag{20}$$

systematically decreases with t. $I_T(q,t)$ is given by eq 17. The shift of q_s can be more explicitly observed in Figure 9 where $S(q,t)$ q^2 at various t's was plotted as a function of q and the crossover q_s at a given t was identified by the arrow. The time change of q_s itself manifests the growth of the domain $\Lambda_m(t)$ and the change of the interfacial structure as discussed in section I. It was plotted in Figure 10 on a double-logarithmic scale. The figure also contains the time evolution of $\Delta\Phi(t)$, which will be fully discussed in the next section. The results clearly show that both $q_s(t)$ and $\Delta\Phi(t)$ undergo a characteristic change at the crossover time t_{cr} (≅270 min) from the intermediate- to the late-stage SD. This t_{cr} is consistent with t_{cr} found by the time-resolved LS experiments. It is quite natural that the domains grow even after $\Delta\Phi(t)$ reaches the equilibrium value. This is a phenomenon relevant to the late-stage SD.

3. Analyses of Internal Scattering $I_T(q,t)$. We analyzed the internal scattering, $I_T(q,t)$, to extract information on $\Delta\Phi(t)$. The principle to determine $\Delta\Phi(t)$ from $I_T(q,t)$ is based upon the following lines of evidence. First, we found $I_T^e(q)$ was successfully described by RPA theory given by eq 9 (see Figures 3 and 4), from which one can determine the volume fraction of one constituent polymer, e.g., ϕ_A, in the single-phase state. Second, $S(q,t)$ for the phase-separating sample at the late-stage SD was found to be successfully described by $S_T(q;T=40\ °C)$ given by eqs 14 and 15 at $q > q_s$ (see Figure 8), from which $\Delta\Phi_e$ can be determined. The same evidence was previously reported by Bates et al.[27] for a well-phase-separated DPB/HPB (protonated polybutadiene) mixture.

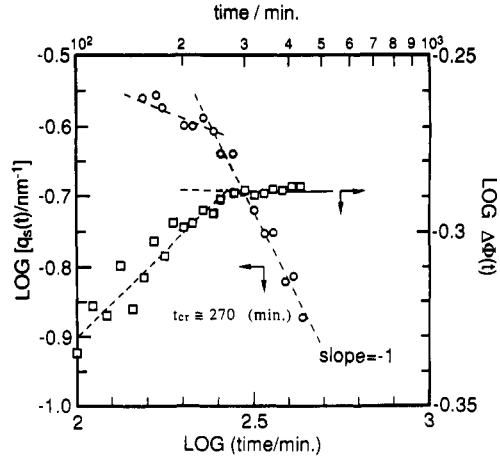

Figure 10. Time change of the crossover wavenumber q_s and the composition difference between the two coexisting phases $\Delta\Phi(t)$ plotted in double-logarithmic scale for H15(HPI)/H18(DPB) (50/50) blend after T-jump from 23 to 40 °C.

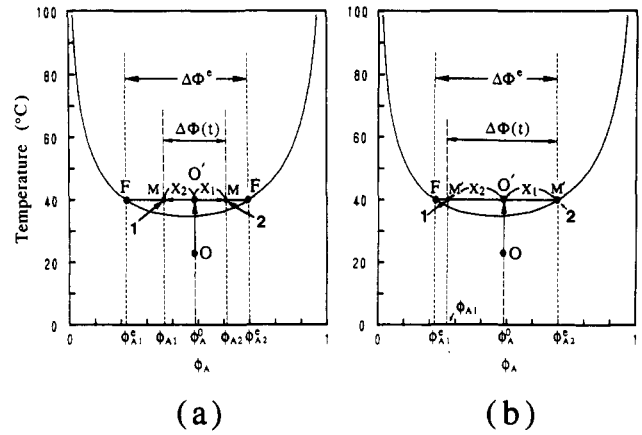

Figure 11. Schematic illustration of the transient process during phase separation induced by quenching the system from point O to O': (a) before phase 2 reaches its equilibrium state and (b) after phase 2 reaches its equilibrium state. The coexistence curves (the solid curves) in parts a and b are identical and were obtained by using the Flory–Huggins theory. Note that there is a slight asymmetry in the coexistence curve as manifested by $\overline{O'M'} \neq \overline{O'F}$.

To extract information on $\Delta\Phi(t)$ in the transient process to achieve $\Delta\Phi_e$, we now applied this principle to the time-resolved SANS profile, $S(q,t)$, by using the internal scattering contribution $I_T(q,t)$ in $S(q,t)$, which was found to be detected at $q > q_s(t)$ in the previous section (eq 20). Figure 11 shows the coexistence curve for this mixture, which was calculated by using the Flory–Huggins theory[28] and the temperature dependence of χ given by eq 6. It schematically illustrates also the transient process induced by quenching the system from point O to O'. The system, which is thermodynamically unstable at O', tends to achieve the equilibrium state F with coexisting phases 1 and 2 having volume fractions of A equal to ϕ_{A1}^e and ϕ_{A2}^e. In the intermediate state M, the domains 1 and 2 have, respectively, volume fractions $X_1(t)$ and $X_2(t)$, compositions (volume fractions of A in each phase) equal to $\phi_{A1}(t)$ and $\phi_{A2}(t)$, and the internal scattering equal to $I_{T1}(q,t)$ and $I_{T2}(q,t)$ (see Figure 11a). Thus the net internal scattering from the system is given by

$$I_T(q,t) = X_1(t)\, I_{T1}(q,t) + X_2(t)\, I_{T2}(q,t) \tag{21}$$

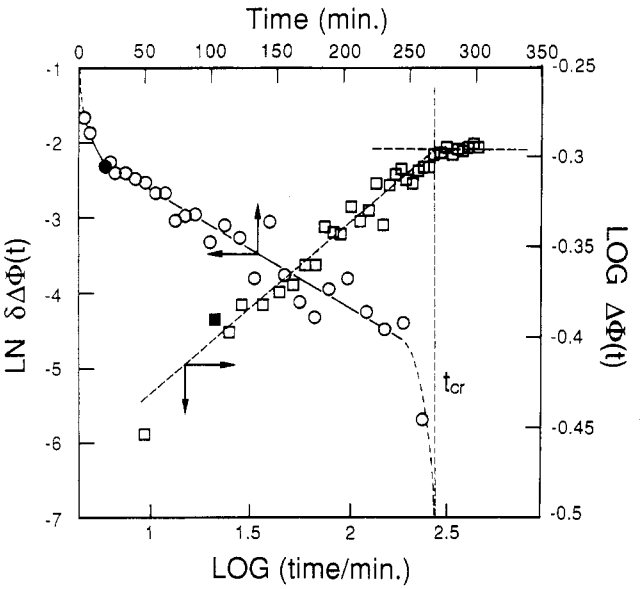

Figure 12. Time change of the composition difference of the two coexisting phases $\Delta\Phi(t)$ and that of $\delta\Delta\Phi(t)$, the difference of $\Delta\Phi(t)$ from the equilibrium value $\Delta\Phi_e$, for a H15(HPI)/H18-(DPB) (50/50) blend after a T-jump from 23 to 40 °C.

with $X_1(t) + X_2(t) = 1$. From eq 9 it follows that

$$I_{TK}(q,t) = \{12\phi_{AK}(t)[1 - \phi_{AK}(t)]/\langle a^2/v\rangle\}q^{-2} \quad (K = 1 \text{ or } 2) \tag{22}$$

where $\langle a^2/v\rangle$ is given by eq 10 with a replacement of ϕ_A by $\phi_{AK}(t)$. In order to determine $\Delta\Phi(t)$

$$\Delta\Phi(t) \equiv |\phi_{A2}(t) - \phi_{A1}(t)| \tag{23}$$

from $I_T(q,t)$ we assume here that

$$X_1(t)/X_2(t) = 1 \tag{24}$$

and that

$$X_1(t)/X_2(t) = [\phi_{A2}(t) - \phi_A{}^0]/[\phi_A{}^0 - \phi_{A1}(t)] \tag{25}$$

Then we only have one adjustable parameter, e.g., $\phi_{A1}(t)$ or $\Delta\Phi(t)$, which can be obtained from $I_T(q,t)$.

When the system reaches an intermediate state M′ as shown in Figure 11b where only domain 2 reaches the equilibrium composition $\phi_{A2}{}^e$, we assume, instead of eqs 24 and 25, that

$$X_1(t)/X_2(t) = [\phi_{A2}{}^e - \phi_A{}^0]/[\phi_A{}^0 - \phi_{A1}(t)] \tag{26}$$

i.e., $\phi_{A2}(t) = \phi_{A2}{}^e$ in eq 25. Note that there is a slight asymmetry in the coexistence curve as manifested by $\overline{O'M'} \neq \overline{O'F'}$.

$\Delta\Phi(t)$ thus evaluated was plotted in Figure 10 together with $q_s(t)$ and replotted in Figure 12 on a longer time scale than in Figure 10. Figure 12 contains the plot of ln $[\delta\Delta\Phi(t)]$ vs t as well as the plot of log $[\Delta\Phi(t)]$ vs log t where

$$\delta\Delta\Phi(t) \equiv \Delta\Phi_e - \Delta\Phi(t) \tag{27}$$

$\Delta\Phi(t)$ appears to increase very rapidly at the initial-stage SD, so that ln $[\delta\Delta\Phi(t)]$ at $t \leq t_1 \cong 19$ min or log $[\Delta\Phi(t)]$ at log $t \leq \log t_1 \cong 1.28$ drops or increases very rapidly with t. Further change of $\Delta\Phi(t)$ appears to be very slow and is approximately described by

$$\Delta\Phi(t) = \begin{cases} \Delta\Phi_e(t/t_{cr})^{0.1} & \text{at } t_1 \leq t \leq t_{cr} \\ \Delta\Phi_e & \text{at } t \geq t_{cr} \end{cases} \tag{28}$$

or

$$\delta\Delta\Phi(t) = \begin{cases} C_1 \exp(-t/\tau) + C_2 & \text{at } t_1 \leq t \leq t_{cr} \\ 0 & \text{at } t \geq t_{cr} \end{cases} \tag{29}$$

where C_1 and C_2 are constants satisfying $\delta\Delta\Phi(t=t_{cr}) = 0$ and $\delta\Delta\Phi(t=0) = C_1 + C_2$, and $\tau = 98$ min at 40 °C or $\Delta T_s = 3.9$ K. It should be noted that at $t \ll t_{cr}$ $\delta\Delta\Phi(t)$ decays exponentially with t

$$\delta\Delta\Phi(t) \cong C_1 \exp(-t/\tau) \tag{30}$$

or the decay rate of $\delta\Delta\Phi(t)$ is proportional to $\delta\Delta\Phi(t)$

$$-\frac{d\delta\Delta\Phi(t)}{dt} \cong \frac{1}{\tau}\delta\Delta\Phi(t) \tag{31}$$

V. Conclusion

Static and time-resolved SANS experiments, which cover the q region satisfying $0.86 < qR_g < 7.8$, were shown to be very useful to the study of the phase transition and later stage spinodal decomposition (SD) of a critical binary mixture of DPB and HPI. SANS profiles $I_T{}^e(q)$ due to the local composition fluctuations in the single-phase state could be quantitatively described by RPA (eq 9 and Figures 3 and 4). This provides a guiding principle to the determination of the time evolution of the composition difference $\Delta\Phi(t)$ in the later stage SD (eq 23 and Figures 10 and 12). The time-resolved SANS profiles, $S(q,t)$, at the early-stage SD ($t < 30$ min) show a crossover behavior in $\partial S(q,t)/\partial t$; the derivative is positive, nearly zero, and negative, respectively, at $q < q^*$ (regime I), $q \cong q^*$ (regime II), and $q > q^*$ (regime III) (see Figures 6 and 7), but the crossover q^* was much larger than the q_c predicted by the linearized theory of SD.[26] $S(q,t)$ at a given t showed the crossover from the domain scattering, $I_d(q,t)$, to the internal scattering, $I_T(q,t)$, with increasing q through the time-dependent crossover wavenumber, $q_s(t)$ (eq 20 in section IV-2 and Figures 8 and 9). The wavenumber, $q_s(t)$, primarily reflects the growth of the global domain structure, $\Lambda_m(t) = 2\pi/q_m(t)$, and hence its time change occurs as a result of the shift of the large q-tail of the domain scattering, $I_d(q,t)$ toward the smaller q region with t. $I_T(q,t)$, which depends on the time change of the local composition $\phi_{A1}(t)$ and $\phi_{A2}(t)$ in domains 1 and 2, allows us to determine $\Delta\Phi(t)$ (eq 21 and Figure 11). Both $q_s(t)$ and $\Delta\Phi(t)$ underwent a characteristic change at the crossover time t_{cr} (≅270 min) from the intermediate to the late-stage SD[2] (Figures 10 and 12 and eqs 28 and 29).

Acknowledgment. We thank Drs. C. J. Glinka and J. Gotaas at the National Institute of Standards and Technology for help with the SANS experiments. This work was supported in part by a Grant-in-Aid for Scientific Research on Priority Areas "New Functionality Materials Design, Preparation and Control" (01604564) from the Ministry of Education, Science and Culture, Japan, and by a scientific grant from the Mitsubishi Foundation, Japan. We thank the Tosoh Co., Ltd., for their gift of the GL4 sample. C.C.H. acknowledges travel support from the National Science Foundation (INT-8915433).

References and Notes

(1) Nose, T. *Phase Transitions* **1987**, *8*, 245. Hashimoto, T. In *Current Topics in Polymer Science*; Ottenbrite, R. M., Utracki, L. A., Inoue, S., Eds.; Hanser: New York, 1987; Vol. II, p 197. Hashimoto, T. *Phase Transitions* **1988**, *12*, 47.

(2) Hashimoto, T.; Itakura, M.; Hasegawa, H. *J. Chem. Phys.* **1986**, *85*, 6118. Hashimoto, T.; Itakura, M.; Shimizu, N. *J. Chem. Phys.* **1986**, *85*, 6773.

(3) Nishi, T.; Wang, T. T.; Kwei, T. K. *Macromolecules* **1975**, *18*, 227. Hashimoto, T.; Kumaki, J.; Kawai, H. *Macromolecules* **1983**, *16*, 641. Synder, H. L.; Meakin, P.; Reich, S. *Macromolecules* **1983**, *16*, 757.
(4) Izumitani, T.; Hashimoto, T. *J. Chem. Phys.* **1985**, *83*, 3694. Takenaka, M.; Izumitani, T.; Hashimoto, T. *Macromolecules* **1987**, *20*, 2257.
(5) Okada, M.; Han, C. C. *J. Chem. Phys.* **1986**, *85*, 5317. Sato, T.; Han, C. C. *J. Chem. Phys.* **1988**, *88*, 2057.
(6) Higgins, J. S.; Fruitwala, H.; Tomlins, P. E. *Macromolecules* **1989**, *22*, 3674.
(7) Higgins, J. S.; Fruitwala, H.; Tomlins, P. E. *Br. Polym. J.* **1989**, *21*, 247.
(8) Schwahn, D.; Springer, T.; Mortensen, K.; Yee-Madeira, H. *Dynamics of Ordering Processes in Condensed Matter*; Komura, S., Furukawa, H., Eds.; Plenum: New York, 1987; p 445.
(9) Schwahn, D.; Yee-Madeira, H. *Colloid Polym. Sci.* **1987**, *265*, 867.
(10) Pyckhout, W.; Schwahn, D.; Sosnowska, I.; Springer, T.; Yee-Madeira, H. *Physica B* **1989**, *156–157*, 402.
(11) Russell, T. P.; Hadziioannou, G.; Warburton, W. K. *Macromolecules* **1985**, *18*, 78.
(12) Meier, H.; Strobl, G. R. *Macromolecules* **1987**, *20*, 649.
(13) Hill, R. G.; Tomlins, P. E.; Huggins, J. S. *Macromolecules* **1985**, *18*, 2555.
(14) Izumitani, T.; Takenaka, M.; Hashimoto, T. *J. Chem. Phys.* **1990**, *92*, 3213.
(15) Hashimoto, H.; Takenaka, M.; Izumitani, T. *Polym. Commun.* **1989**, *30*, 45. Takenaka, M.; Izumitani, T.; Hashimoto, T. *J. Chem. Phys.* **1990**, *92*, 4566.
(16) Tomlins, P. E.; Higgins, J. S. *J. Chem. Phys.* **1989**, *90*, 6691.
(17) Bates, F. S.; Wiltzius, P. *J. Chem. Phys.* **1989**, *91*, 3258.
(18) Ohta, T.; Nozaki, H. In *Space-Time Organization in Macromolecular Fluids*; Tanaka, F., Doi, M., Ohta, T., Eds.; Springer: *Tokyo*, 1989; p 51.
(19) Nose, T. Reference 18; p 40.
(20) Chakrabarti, A.; Toral, R.; Gunton, J. D.; Muthukumar, M. *Phys. Rev. Lett.* **1989**, *63*, 2027.
(21) Hashimoto, T.; Hasegawa, H.; Takenaka, M.; Jinnai, H.; Sakurai, S.; Han, C. C. Proceedings of the International Conference on Polymer Research by Neutron Scattering, The Taniguchi Conference, Division of Polymer Chemistry, Nov 7–9, 1989, Kyoto, Japan, to be submitted to *Macromolecules*.
(22) de Gennes, P.-G. *Scaling Concepts in Polymer Physics*; Cornell University Press: Ithaca, NY, 1979.
(23) Glinka, C. J.; Rowe, J. M.; LaRock, J. G. *J. Appl. Crystallogr.* **1986**, *19*, 427.
(24) Glinka, C. J.; Krueger, S. NBS Memorandum for SANS Users, Dec 29, 1986.
(25) Shibayama, M.; Yang, H.; Stein, R. S.; Han, C. C. *Macromolecules* **1985**, *18*, 2179.
(26) Cahn, J. W. *J. Chem. Phys.* **1965**, *42*, 93.
(27) Bates, F. S.; Dierker, S. B.; Wignall, G. D. *Macromolecules* **1986**, *19*, 1938.
(28) Flory, P. J. *Principles of Polymer Chemistry*; Cornell University Press: Ithaca, NY, 1953.

Registry No. DPB, 9003-17-2; HPI, 9003-31-0; neutron, 12586-31-1.